Superconductivity

Mähring, Marcus[1]

[1]ETH Zürich
December 24, 2021

Abstract

In this experiment the phenomenology of superconductivity is investigated. This is done by measuring the magnetization curve of three different superconductors, one type-I (Pb) and two type-II superconductors (Pb5%In, and Pb7%In). This is done by cooling them below their critical temperatures using liquid helium and nitrogen to insulate them from the outside environment using a cryostat. In this cryostat an external magnetic field is applied on the measurement assembly from which the magnetization as a function of the H-field can be measured. Ultimately, the condensation energy, energy band gap, and the Ginzburg-Landau-parameters where applicable. The curve for the third sample was distinctly different from the first two, most probably stemming from an error in the measurement process and insufficient calibration. Ultimately, the given values seemed to provide a faithful representation of the samples' superconductivity. Additionally, some parts of superconductivity theory are discussed in relation to their subtle appearance in the data.

Contents

1 Introduction **3**
1.1 Phenomenology . . . 3
1.1.1 Type-I and type-II superconductors . . . 3
1.2 Descriptions . . . 4
1.2.1 London Theory . . . 4
1.2.2 Ginzburg-Landau Theory . . . 4
1.2.3 BCS Theory . . . 5

2 Experiment **6**
2.1 The cryostat . . . 6
2.2 Vacuum pumping the cryostat . . . 6
2.3 Cooling the cryostat . . . 7
2.4 Pick-up Coil . . . 7
2.5 Calibration . . . 7
2.6 Measuring the superconductivity . . . 8

3 Results **9**

4 Data analysis **10**
4.1 Feature identification . . . 10
4.2 Conversion to H-field . . . 10
4.3 Calibration and further correction . . . 10
4.4 Determining critical temperature for the type-II superconductors . . . 11
4.5 Condensation energy and energy gap . . . 12
4.6 Calculating the Ginzburg-Landau-parameter . . . 12
4.7 Calculating the derivative of the magnetisation curves . . . 13

5 Discussion **15**

6 Conclusion **16**

A Safety **17**

1 Introduction

Superconductors and superconductivity phenomena has since their advent revolutionized several fields and wrought technologies in all aspects of modern life. From medicine with magnetic resonance imaging, particle accelerators with the LHC, and possible future modes of transportation a revolution in the field of superconductors would be hugely important. To this end, this report aims to understand some elementary phenomenology and theory of superconductors, as well as investigating three superconductors and their properties [1].

1.1 Phenomenology

Generally, superconductors are a subset of materials where the electrical resistance drops to 0 after being cooled to a critical temperature T_c specific to the material. Additionally, these materials possess a critical magnetic field H_c, a threshold after which it ceases to superconduct. The equation describing this phenomenon is [2]:

$$H_c(T) = H_c(0)\left[1 - \left(\frac{T}{T_c}\right)^2\right] \tag{1}$$

In a thermodynamic sense, superconductivity can be regarded as a phase of matter with a continuous phase transition. From the fact that electrical resistance vanishes, one can also find via the Maxwell equations, that the magnetic field must vanish in a superconductor, $\mathbf{B} = 0$. This is called the *Meissner-Ochsenfeld* effect which enables magnetic levitation above a superconducting object [2].

A superconductor has perfect diamagnetic behaviour:

$$\mathbf{M} = -\mathbf{H}_a \tag{2}$$

with $\mathbf{H}_a$ being the applied external field and $\mathbf{M}$ the magnetisation [2].

1.1.1 Type-I and type-II superconductors

There are two main classes of superconductors, called type-I and type-II conductors respectively. Pure samples are mostly type-I conductors while alloys are mostly type-II. In the absence of an external magnetic field, type-I and type-II superconductors have similar properties, but if a strong magnetic field is applied they undergo different processes. A type-I superconductor is abruptly destroyed, while a type-II conductor reaches a first critical temperature where the entire magnetic field can no longer be expelled, H_{c1}, but remains superconducting. After a second critical value is reached, the superconductivity is broken, H_{c2}.

Another way of categorizing superconductors is if they are a *low-temperature superconductor* (LT) *high-temperature superconductor* (HT), with HT conductors having critical temperatures $T_c > 23\,\mathrm{K}$ [2].

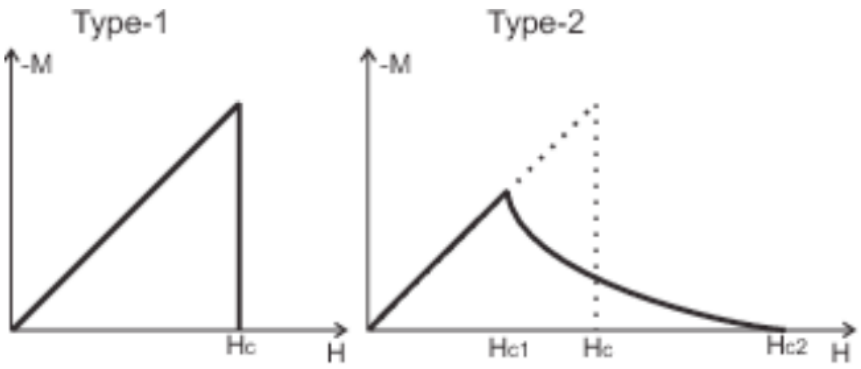

Figure 1: Caption

1.2 Descriptions

1.2.1 London Theory

The suppression of the magnetic field inside a superconductor cannot extend to the boundary of the superconductor, as it would lead to a discontinuity in the magnetic field at the interface. London theory describes this phenomenon via two main equations:

$$\frac{\partial \mathbf{j}}{\partial t} = \left(\frac{nq^2}{m}\right)\mathbf{E} \tag{3}$$

$$\nabla \times \mathbf{j} = -\left(\frac{nq^2}{m}\right)\cdot \mathbf{B} \tag{4}$$

with $\mathbf{j}$ the current density. The second equation leads to the Meissner-Oschenfeld effect. Together with the Maxwell equations one can derive the *London penetration depth*:

$$\lambda_L = \sqrt{\frac{m}{\mu_0 n q^2}} \tag{5}$$

where $n = n(T)$ is the charge carrier density [2].

1.2.2 Ginzburg-Landau Theory

The Ginzburg-Landau theory examines superconductors through the lens of thermodynamics. Defining $n_s(T)$ as the density of superconducting charge carriers and the order parameter Ψ with $|\Psi|^2 = n_s^2$. When $\Psi = 0$ we are in the normal state and when $\Psi \neq 0$ is the superconducting state, which is only available at $T < T_c$ [2].

From the theory one may also derive the Ginzburg-Landau equations from which the penetration depth can be re-derived. From this, the decay of density of the superconducting charge carriers is given by:

$$\xi = \sqrt{\frac{\hbar^2}{2m|\alpha|}} \tag{6}$$

This only holds for type-I superconductors. Here α is the scaling of the density of superconducting states to the free energy. Hence, the Ginzburg-Landau parameter can be defined [2]:

$$\kappa = \frac{\lambda_L}{\xi} \tag{7}$$

1.2.3 BCS Theory

BCS theory was the first theoretical microscopic description of superconductivity and relies on spin-singlet states acting as bosons to circumvent the Pauli exclusion principle. In BCS theory it can be derived that the critical magnetic field is given by

$$H_c = \lambda_L \cdot j_c \approx \lambda_L \frac{e n_s \Delta}{\hbar k_F} \tag{8}$$

with k_F being a constant for the fermi energy, Δ the dependent energy gap in the excitation spectrum from the superconductor and λ_L being the penetration depth.

A direct result from the theory is that the condensation energy can be connected to the condensation energy of Cooper pairs via:

$$E_{con} = \frac{\mu_0 H_c^2}{2} = -\frac{1}{2} Z(E_F) \Delta^2 \tag{9}$$

with $Z(E_F) = D(E_F)/2$ is half the density of states at the Fermi energy for the free electron gas. We divide by two to only consider Cooper-pairs [2]. The density of states is given as follows [1]:

$$D(E) = \frac{m_e}{\pi^2 \hbar^2} \sqrt{2 m_e E} \tag{10}$$

where m_e denotes the electron mass. For lead, the Fermi energy is given as $E_{F,Pb} \approx 9.47\,\mathrm{eV}$ [3]

The BCS theory also gives a result for type-II which links the Ginzburg-Landau-parameter to the critical magnetic fields [2]

$$\frac{\lambda_L}{\xi} = \kappa = \sqrt{\frac{H_{c2}}{2 H_{c1}}} \tag{11}$$

2 Experiment

To observe superconductivity for the investigated samples, they need to be cooled to a few Kelvin. This is done by putting the samples in a container surrounded by liquid helium. The helium is additionally isolated by a chamber containing liquid nitrogen and two vacuum chambers.

2.1 The cryostat

The cryostat is a multilayered chamber in which the sample can be cooled to a very low temperature while being subjected to an external magnetic field. This cryostat is made out of four compartments. The first layer is a vacuum insulation layer which divides the experiment from external temperatures. The second layer is a chamber which is filled with liquid nitrogen, which stabilizes at 77 K. Within this layer is another vacuum layer which again insulates the innermost chamber. The final chamber is filled with liquid helium. Around the innermost part of the compartment a solenoid with 4008 windings which was 15 cm long. is coiled, allowing the application of an external magnetic field.

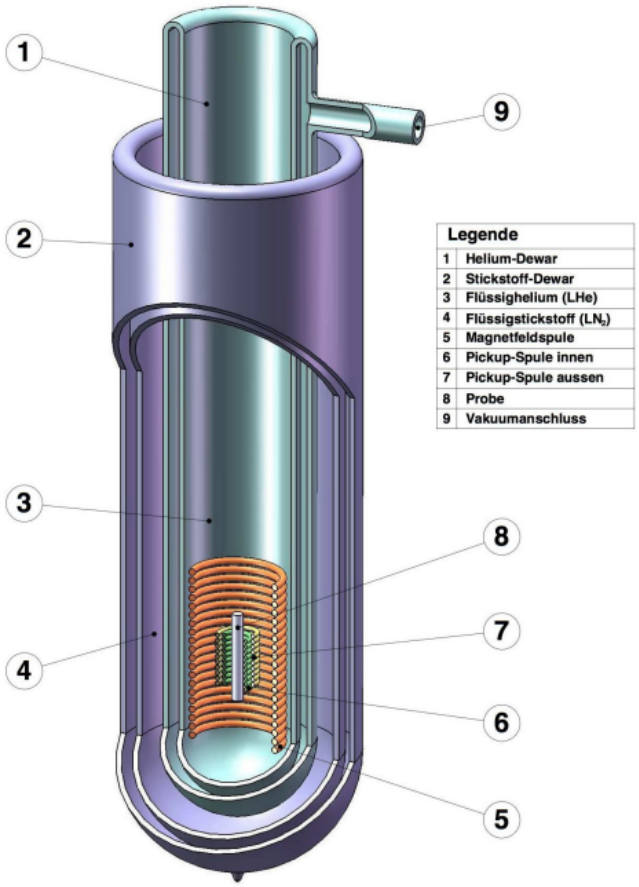

Figure 2: The cryostat used during the experiment with annotation of the different components.

2.2 Vacuum pumping the cryostat

Before undertaking the experiment, the inner vacuum chamber must emptied to ascertain proper isolation of the liquid helium. Firstly one needs to close all the valves, whereafter one turns on

the pump. Then one carefully opens the valves from the pump to the inner chamber. All valves are then closed half-way to relieve the stress on them.

The pump was then left for two days to induce the vacuum. Ultimately, when the experiment was performed, the pressure had reached 0.03 mbar. There was no indication of a leak in the vacuum system, so the valves were closed starting at the cryostat toward the pump, after which the pump was turned off.

2.3 Cooling the cryostat

In the next step about 10 L of liquid nitrogen were retrieved from the central reservoir and used to fill the second chamber. This was indicated by the fizzing at the top of the chamber which got louder when the chamber was almost filled.

Finally, a dewar filled with liquid helium was connected to a recollection line to reduce cost and then connected to the experiment. Then the liquid helium was slowly pumped over to the cryostat by inducing a pressure gradient with the help of the recollection line. During the experiment the second chamber was continuously topped of.

To see the progression of the liquid helium while filling the chamber up a high intensity light source and a hair-dryer were used to better see the helium surface and the remove condensation from the window through which one could view them.

Then the rod where the sample was to be attached was slowly inserted in the liquid helium over a ten minute interval, letting the fumes from the condensating helium cool it. This was done to ensure that all helium did not boil of before the measurements could be performed.

2.4 Pick-up Coil

The pickup coil system measures the magnetization of the sample. It consists of two coils which are oppositely wound in a casing on the end of a long round. The warm assembly was then inserted *very slowly* into the cryostat. See figure 3 for a detailed view.

The circuit itself is made out of an inner coil which surrounds the sample and an outer coil surrounding the inner coil. The coils are cocentric and oppositely wound. Additionally in series a variables resistor with a constant resistance is connected.

2.5 Calibration

Before collecting data, background calibration need to be performed, which is done without a sample. The point of the calibration is to certify that the voltage drop between point 1 and point 2 (1 is between the two parts of the variables resistor and 2 is between the two coils) remains about zero. This is done by adjusting a values of the two variable resistors of the potentiometer.

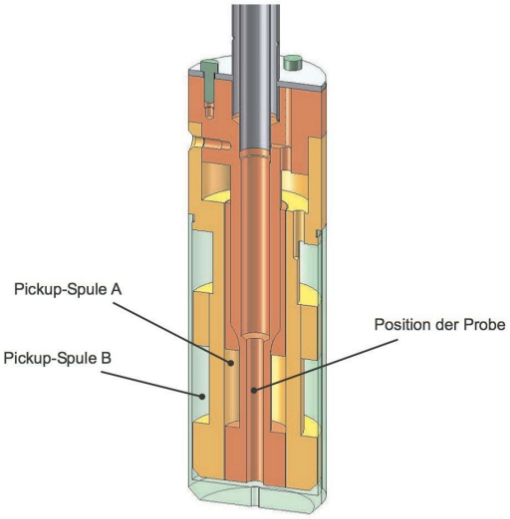

Figure 8: Detailed cross section of the sample stage.

Figure 3: The sample within the pickup coil with the outer coil wrapped around on the outside.

2.6 Measuring the superconductivity

Before measuring a 50 mΩ resistor was put into series with a magnet and the current source. Then the magnetization was measured in the following way:

The voltage drop across the precision resistor was then measured and was recorded using Labview, with the potentiometer and coils in series. Point 1 and 2 are then fed to an integrator which is output to the computer.

Before recording the samples, they had to be pre-cooled in liquid nitrogen. Afterwards the sample was attached to the sample rod, and was slowly inserted over a 60 s interval to avoid bending or deformation of the samples. When attaching and detaching samples one also needed to be quite careful to not destroy the samples.

3 Results

In figure 1 the chosen calibration curve is displayed. Note how the recorded values are time, the voltage drop between the two points, and finally the integrated voltage from the integrator.

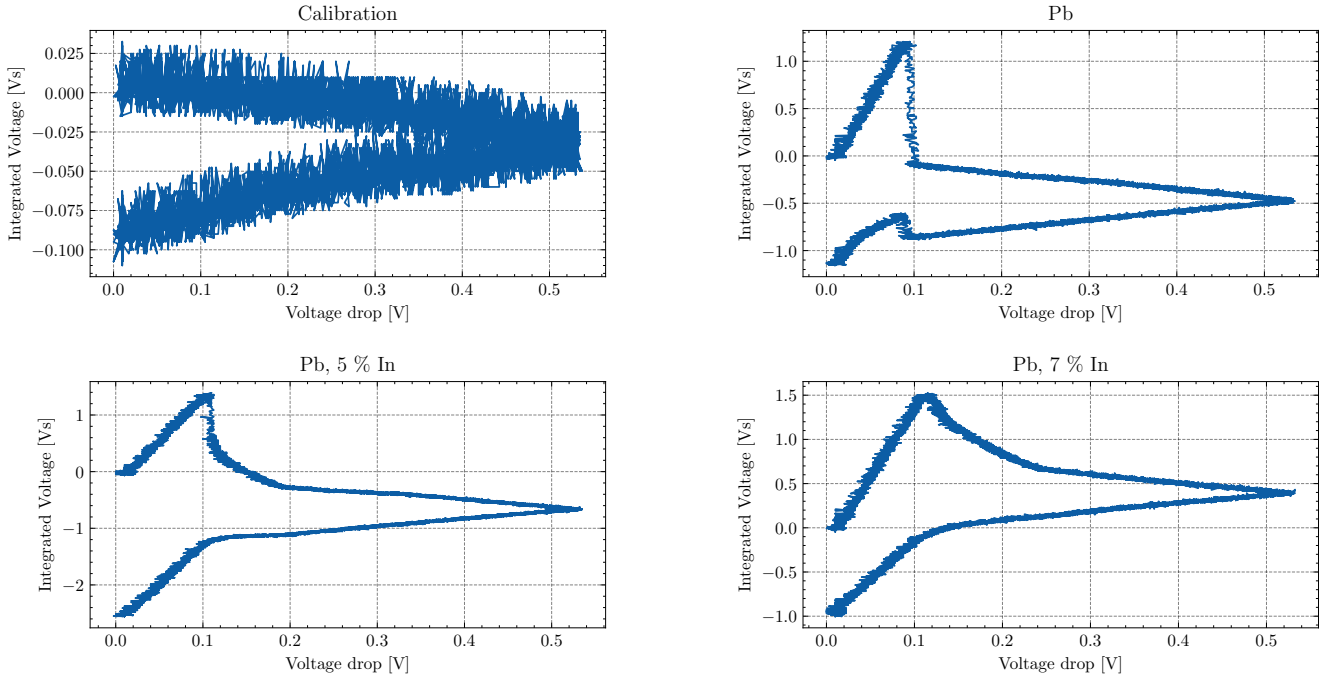

Figure 4: The results from the experiment showing the integrated voltage over the recorded period.

The voltage drop can be converted to the current itself using Ohms law:

$$I = \frac{V_{drop}}{R} \tag{12}$$

with R being the precision resistor of $50\,\mathrm{m\Omega}$.

4 Data analysis

4.1 Feature identification

For the data analysis the curves were recalibrated using the calibration data set, which was done by subtracting it from the data. Due to this fact, from this point on, only the three points of interest will be shown. Additionally, as the analysis is only performed until the polarity of the current was reversed, the subsequent plots will only show this part.

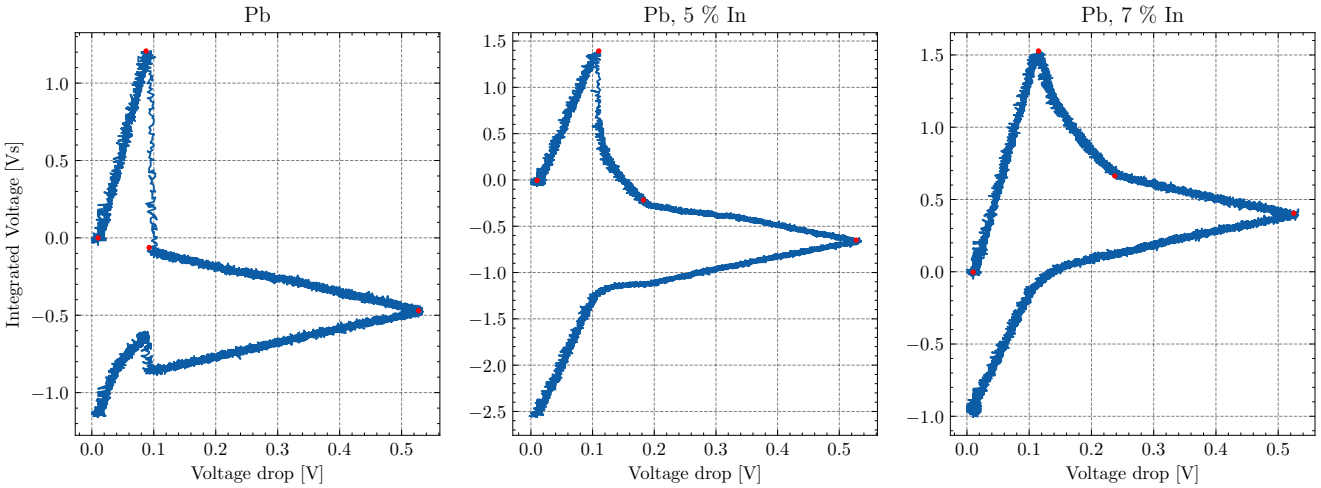

Figure 5: The data sets of the different samples with red dots marking the spots of interest. These will turn out to either be areas

4.2 Conversion to H-field

The real analysis is performed in several steps, first we choose to convert the x-axis into the externally applied H-field (also proportional to to the current). This is done by using the following formula for a magnetic field of a solenoid:

$$B = \mu_0 \frac{NI}{\ell} \tag{13}$$

where N is the amount of windings of the coil, I is the current flowing through it, and ℓ is the length. Plugging in the formula from the voltage drop and the definition of the H-field we use the relation $B = \mu_0 H$ to get:

$$H = \frac{NV_{drop}}{Rl} \tag{14}$$

ignoring the magnetization which we then measure. Here we use the voltage drop through the precision resistor to get a better value for the current.

4.3 Calibration and further correction

The rest of the data analysis starts by cleaning the data further an particularly correcting some curves. Firstly, the magnetization of the sample needs to reach zero after the last critical H-field value (for type-I this is of course only H_c but for type-II it is H_{c2}). Then, the x-axis needs

recalibration once more to impose the norm slope. The fit we do to correct for slope is strictly linear, as we don't want to displace the zero of the data set.

To perform this normalization of the curve, we first need to find some points between the correction fits can be performed, namely in the area after the final critical value. In figure 6 this is done with the points found previously which shall be used throughout the analysis with the subsequent errors discussed here.

Note the poor fit for the 7% In sample which will be discussed later.

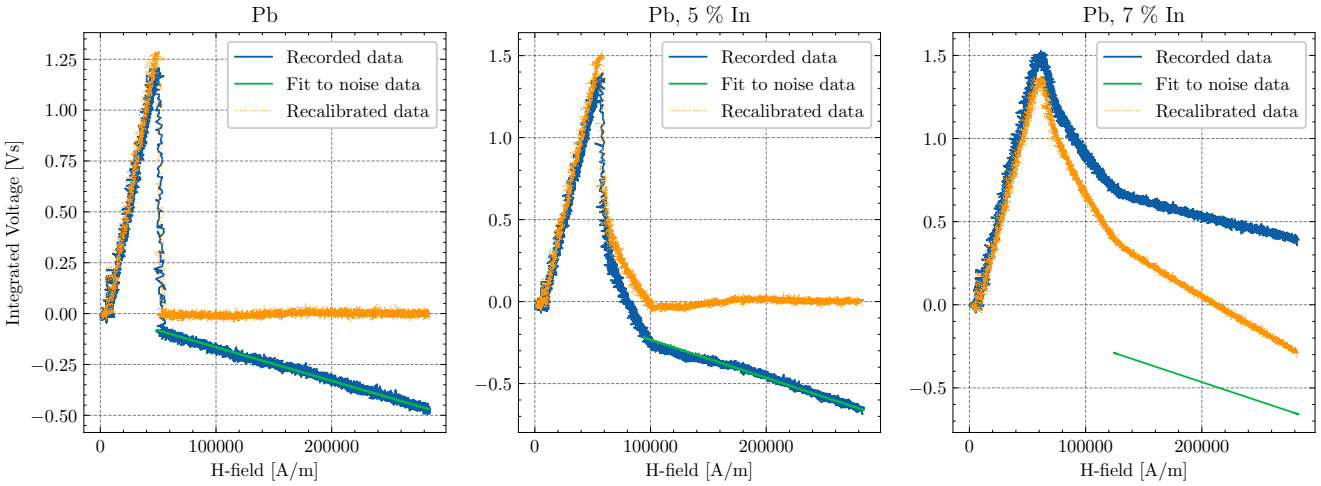

Figure 6: Caption

They are listed in table 1 for convenience as later also turn out to correspond to the critical magnetic fields.

Sample	Hc	Hc1	Hc2
Pb	50768 ± 4008		
Pb5%In	96043 ± 2881	58784 ± 2672	97528 ± 4008
Pb7%In	114772 ± 3443	61456 ± 2672	126920 ± 4008

Table 1: The critical H-field values for the different samples, were applicable. The calculation of H_c for the type-II superconductors is explained in the following section.

Thereafter a unit conversion was performed to convert the voltage drop to the magnetization. This is done by utilizing equation (2) and enforcing the initial slope between the magnetization and H-field before reaching a critical value need be the identity. This recalibration can be seen in figure 7.

4.4 Determining critical temperature for the type-II superconductors

From this point onward the data is cleaned and the substantial analysis can be performed. In a first step we calculate H_c for the two type-II conductors by observing from figure 1 that the following relation must hold:

$$\frac{H_c^2}{2} = \int_0^{H_{c2}} \text{type-II curve} \tag{15}$$

with the left hand side stemming from the area of a triangle. In figure 8 the finished calibrations together with the critical values are given.

The numerical integration was done using the Trapez rule.

4.5 Condensation energy and energy gap

Now, the condensation energy and the corresponding energy gap shall be determined. The condensation energy is according to equation (9) given by the expression:

$$E_{Con} = \frac{\mu_0 H_c^2}{2} \tag{16}$$

and the energy gap can be derived from this via:

$$\Delta = \sqrt{2\frac{E_{Con}}{Z(E_F)}} \tag{17}$$

Which leaves us with the values in table 2.

Sample	Condensation energy [J]	Energy gap [μJ]
Pb5%	5795.83 ± 347.75	257.55 ± 7.73
Pb7%	8276.55 ± 496.59	307.77 ± 9.23

Table 2: Condensation and energy gap for the applicable samples.

4.6 Calculating the Ginzburg-Landau-parameter

At this point the Ginzburg-Landau-parameter (equation (11)) is calculated for the type-II conductors. Results in 3.

Sample	Ginzburg-Landau
Pb5%	0.911 ± 0.028
Pb7%	1.016 ± 0.027

Table 3: The Landau-Ginzburg parameter for the two samples.

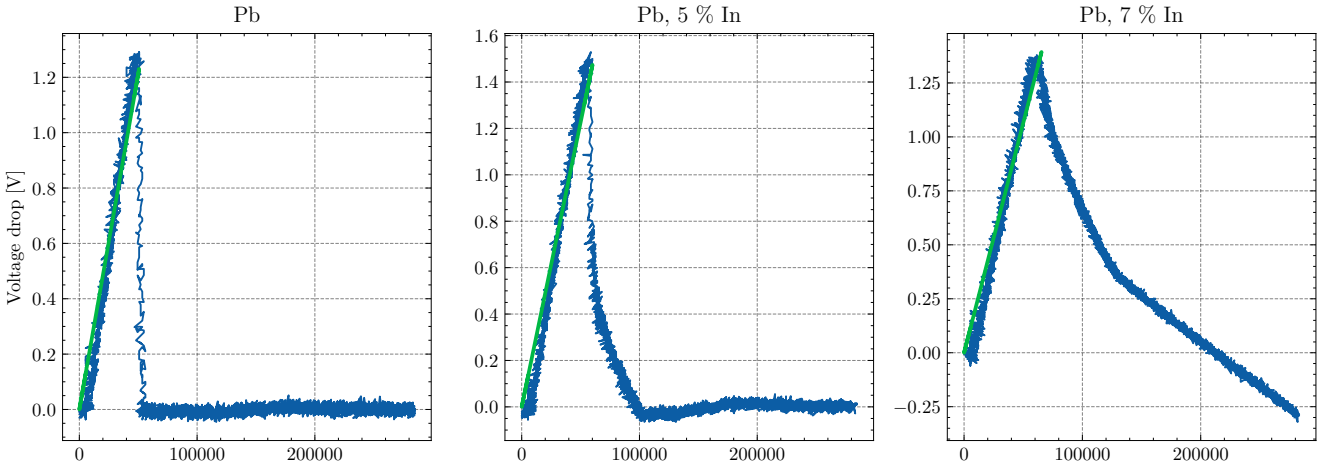

Figure 7: The data set before undergoing unit correction with a fitted green curve describing the correction slope which was then applied.

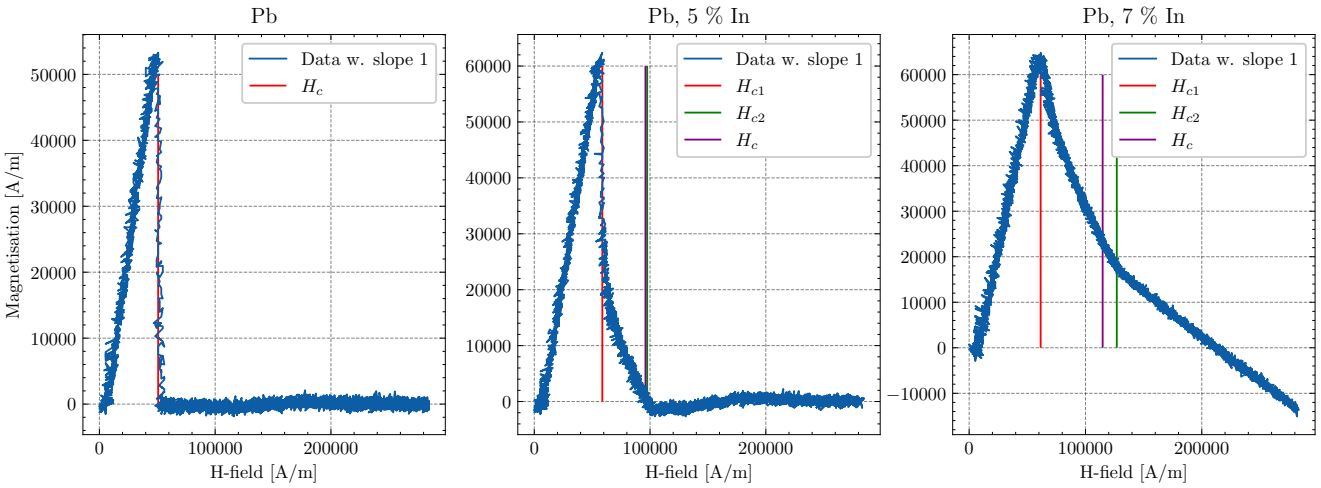

Figure 8: The data sets post-calibration with the different critical H-field values marked in the data sets.

4.7 Calculating the derivative of the magnetisation curves

Finally the expression

$$\frac{1}{H_{c2}}\left(\frac{\partial M}{\partial H}\right) \tag{18}$$

is calculated for the two type-II conductors. We know this value will correspond to H_{c2}^{-1} for $H < H_{c1}$ and 0 for $H > H_{c2}$ meaning the only region of interest is $H_{c1} \leq H \leq H_{c2}$. These curves were fitted to get a derivative, and can be found in figures 9. Finally the derivatives through the second critical values are given in 10.

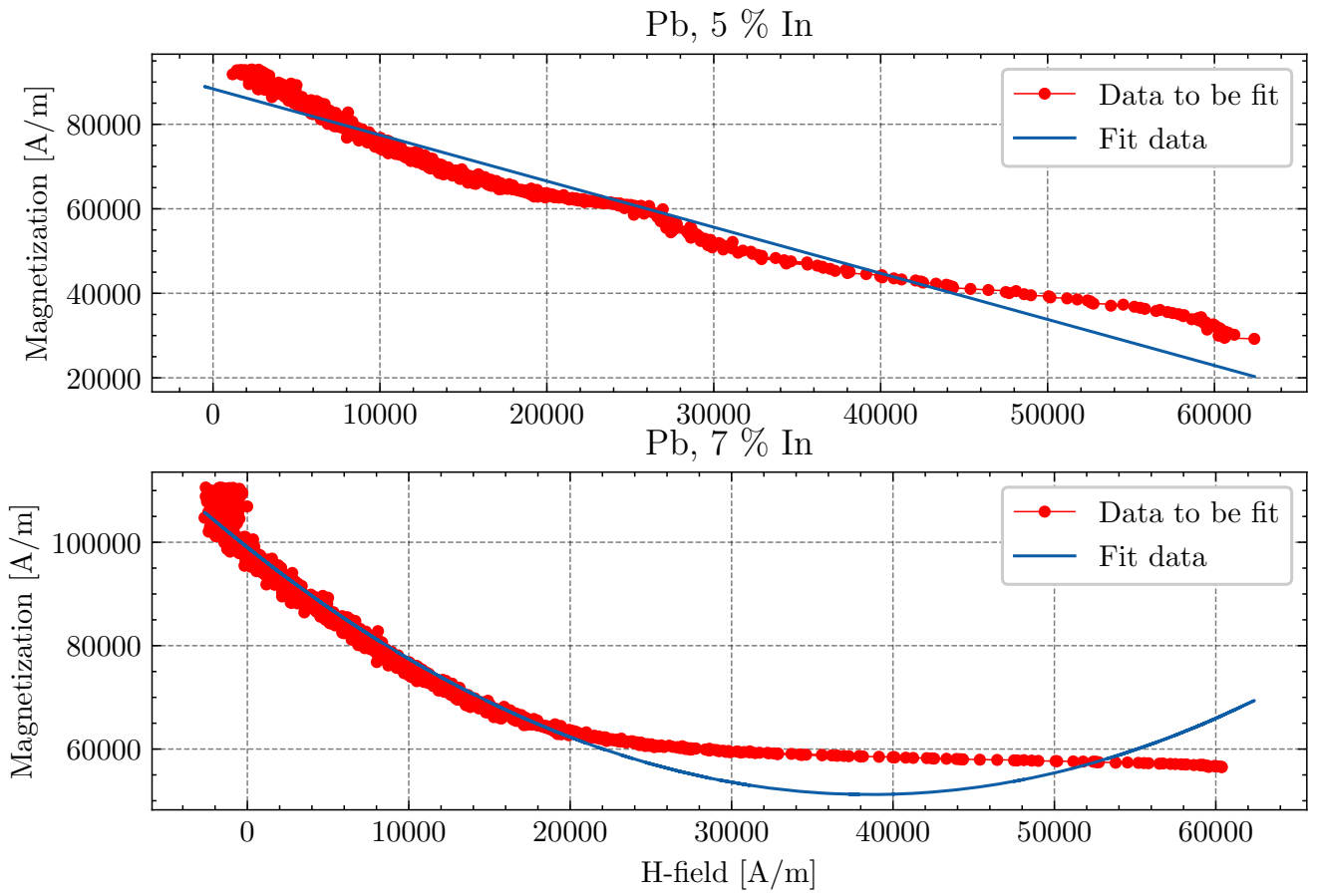

Figure 9: Two fits for the different curves in the region of interest.

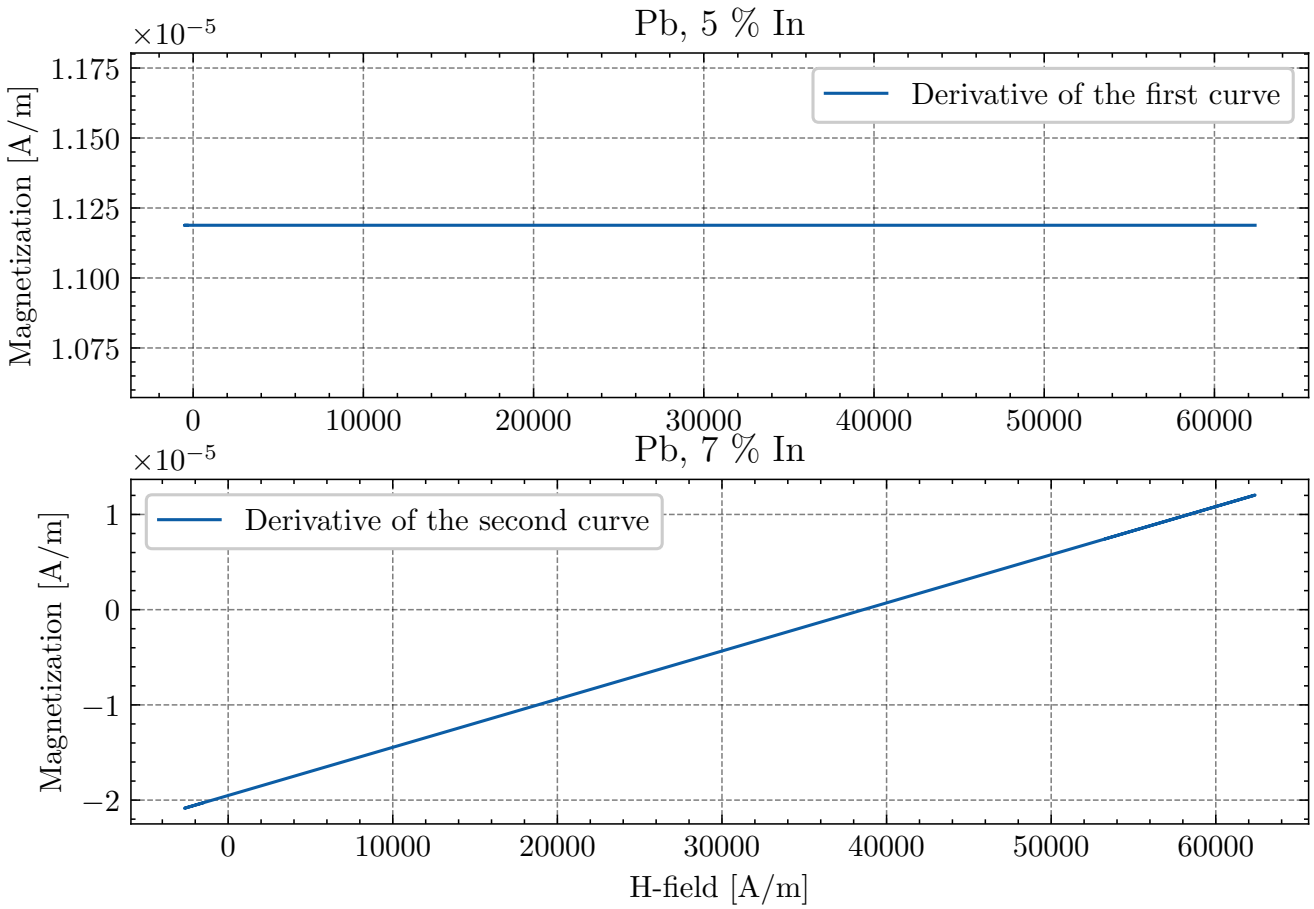

Figure 10: The derivatives at these points divided through the final critical H-field value.

5 Discussion

Firstly we briefly explain the magnetic levitation phenomenon seen in figure 2 of the experiment manual [2]. The second London equation stipulates:

$$\vec{\nabla} \times \vec{j_s} = -\frac{n_s e^2}{m} \vec{B} \tag{19}$$

with $\vec{j_s}$ is the superconducting current density and m is the electron mass [4]. This describes how the B-field within a superconductor becomes expelled and bent around it, meaning the superconductor becomes highly diamagnetic, meaning it's repelled by a magnetic field. This force can be stronger than gravity if a sufficiently strong magnetic field is applied, explaining the Meisner-Ochsenfeld effect.

The traces for type-I superconductors are softer peaks than the image shown in figure 1. This lesser decrease of the magnetization above H_c than expected. This stems from the demagnetization field of the samples, which is an extra term in the description of how the magnetization leads to additional boundary conditions [4].

The magnetization also shows extensive hysteresis which is most likely an effect from magnetic hysterisis and vortices in the superconductors: an effect were tubes of magnetic flux penetrate the material [5]. This could induce a certain amount of resilience to outer magnetic fields when they temporarily reach some equilibrium of the amount of cooper pairs traveling through the samples.

The values all look reasonable for the samples, even for the second type-II superconductor with 7%In, even though the fits are shifted. This stems from the fact that the values are mostly positive and the fit completely linear. The fit per se is not bad to the overall slope, but considering that unlike the two previous samples, the final sample did go under zero before the polarity switch. This could have been due to the fact that the helium levels were quite low at this point, and that the final measurement was done twice. Once without showing any reaction in the circuit, most likely stemming from the sample not having reached its critical temperature. To counteract this, author under supervision of the assistant tweaked the calibration, but after it was found that the problem had disappeared, a recalibration was not performed. It is also possible that the polarity switch happened to late or some part of the equipment was altered during the troubleshooting process. Nevertheless, the retrieved values seem reasonable and indeed the features could be identified. A significant caveat here is that the values here are going to be skewed, due to the insufficient calibration. This should be improved in the future.

Another note from the experiment is that the energy gaps are much larger than the author first suspected, being about 10 orders of magnitude greater than the band gap in a semiconductor.

6 Conclusion

In conclusion, this experiment investigated the magnetization curves of one type-I and two type-II superconductors. In the experiment condensation energy and the energy gap were determined for all samples, as well as the critical H-field values for the magnetization curves. The values turned out to be mostly reasonable, but with higher values then expected for the energy band gap.

A Safety

The experiment should be performed under the supervision of an assistant due to the danger and complexity of working with liquid helium.

Additionally, when operating the container with the liquid nitrogen gloes and safety goggles should be worn at all times. Connections, pipes, and other equipment in contact with the cryofluids should also never be touched without gloves, as this can easily lead to cold burns. As always closed shoes should be warn to prevent splattering of nitrogen onto exposed skin.

Lastly, the samples are made out of heavy metals and should not be handled directly.

References

[1] Charles Kittel. *Einführung in die Festkörperphysik*. Oldenbourg Wissenschaftsverlag, 2013. Original title: Introduction to solid state physics.

[2] Philip Maechler (2009) and M. Leopold (2011). Superconductivity. `https://vp.phys.ethz.ch/Experimente/pdf/Superconductivity.pdf`. Accessed: 22.11.2021.

[3] Neil W Ashcroft, N David Mermin, et al. Solid state physics, 1976.

[4] Harald Ibach and Hans Lüth. *Festkörperphysik: Einführung in die Grundlagen*. springer-verlag, 2009.

[5] Jennifer Deang, Qiang Du, Max Gunzburger, and Janet Peterson. Vortices in superconductors: modelling and computer simulations. *Philosophical Transactions of the Royal Society of London. Series A: Mathematical, Physical and Engineering Sciences*, 355(1731):1957–1968, 1997.